Modelling of crack propagation in miniaturized and normal SENB specimens based on local failure criterion

Bernadett Spisák, Szabolcs Szávai
Bay Zoltán Nonprofit Ltd. for Applied Research, University of Miskolc, Hungary
bernadett.spisak@bayzoltan.hu, https://orcid.org/0000-0001-8003-3117
szabolcs.szavai@bayzoltan.hu, https://orcid.org/0000-0002-8311-2870

Zoltán Bézi, Réka Erdei
Bay Zoltán Nonprofit Ltd. for Applied Research, Hungary
zoltan.bezi@bayzoltan.hu, reka.erdei@bayzoltan.hu

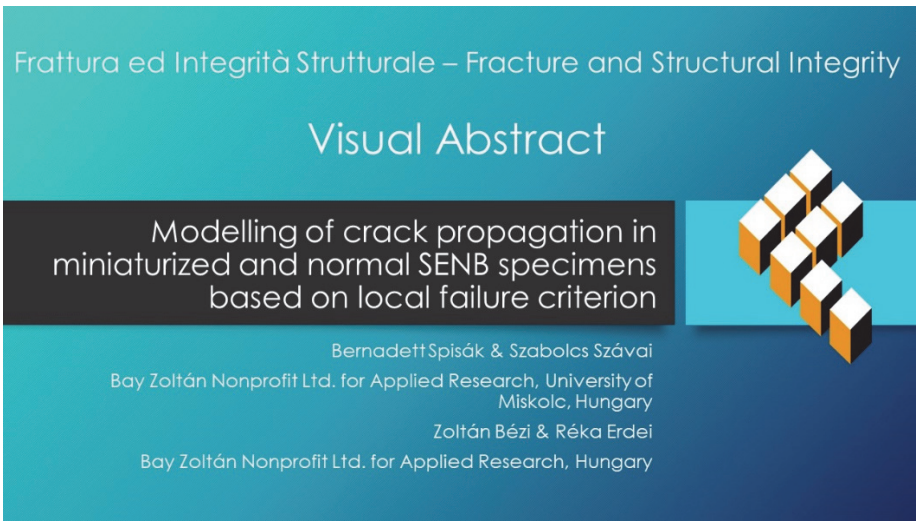

Citation: Spisák, B., Szávai, S., Bézi, Z., Erdei, R., Modelling of crack propagation in miniaturized and normal SENB specimens based on local failure criterion, Frattura ed Integrità Strutturale, 68 (2024) 269-309.

Received: 17.01.2024
Accepted: 10.02.2024
Published: 27.02.2024
Issue: 04.2024

KEYWORDS. GTN model, ANN method, VCCT (virtual Crack Closure Technique), Fracture toughness, Fracture mechanics.

INTRODUCTION

Reactor pressure vessels (RPV) are key parts of nuclear power plants (NPPs). The fracture toughness of RPV vessel beltline materials is continuously monitored throughout the lifetime of the nuclear power plant to guarantee the smooth operation of the plant. The base material of RPVs is ferritic steel, which undergoes ductile fracture at elevated temperatures and brittle fracture at lower temperatures. It also should be noted, that the transition from ductile to brittle behavior is shifted to higher temperatures when these steels are subjected to neutron irradiation. In order to ensure

that ferritic steels preserve sufficient structural integrity at service temperatures, actual RPV materials are used in monitoring programs that provide an assessment of toughness behavior over their service life. These monitoring programs were initially based on impact energy measurements of Charpy specimens. However, Charpy tests cannot directly measure the fracture toughness of the material. The amount of material required for accurate characterization of ductile-brittle transition region (DBTR) for fracture analysis is sometimes limited. However, nuclear power plants usually have many irradiated and previously tested Charpy specimens, so further investigations can be performed by cutting up them. Such tests can be carried out with mini CT specimens, as up to eight of them with 4 mm thickness can be produced from a single Charpy specimen [1].

In addition to investigating RPVs, miniaturized specimens can also be used to determine the fracture toughness of many other components. For example, Bao et al. [2] in order to overcome the limiting dimensions of welded metal and heat affected zone regions, used miniature SENB specimens to perform fracture toughness tests.

The simulation of the brittle-ductile transition zone is still not yet solved. The main concept of this research work is to combine a brittle and ductile model, so during the simulation, the driving force of the crack propagation could change based on which type of fracture mechanism is more dominant. Subsequently, simulations should be performed at several temperature levels. For the ductile damage model, the well-known Gurson-Tveergard-Needleman (GTN) model was chosen [3], [4].

One of the main advantages of the VCCT model [5] is that the crack does not propagate when elements are removed from the simulation but opens the mesh when the set limit is reached. The method was originally developed for the simulation of brittle fractures, where the fracture criterion is defined as the limit of the strain energy accumulated at the crack tip, but its finite element representation allows the simulation of ductile crack propagation. An important step in the model development was to investigate how the advantages of the GTN and VCCT techniques can be applied in a model to determine the J_Q fracture toughness value of a given material as accurately as possible using simulation tools. In the followings, the modification of the VCCT method is going to be introduced, which at the moment can be used for the determination of J_Q in the ductile region. The article contains the second step of the validation procedure, where miniaturized and normal SENB specimens were investigated.

OVERVIEW OF GURSON-TVERGAARD-NEEDLEMAN MODEL

In case of fracture mechanics two approaches are distinguished: the global and the local approach. The global approach assumes that the fracture toughness can be described by a single parameter. Furthermore, it does not pay attention to the micro-mechanisms of failure. In addition, the parameter defined depends on the size of the sample, which makes the transferability of laboratory measurements to large-scale equipment problematic. This is the reason why the local approach to fracture is an area of increasing research [6].

For the local approach, fracture toughness modelling is based on local fracture criteria, which are subsequently applied to the crack tip. The advantage of this method is that the criteria thus defined depend only on the material and not on the geometry, which ensures that the measurement results can be implemented in large-scale equipment tests [7], [8]. It can also be used when only a small amount of material is available. The identification and determination of micromechanical parameters requires a combination of laboratory tests and numerical simulations. The basic structure of the model most commonly used to describe plastic deformation was described by Gurson in 1977 [3]. In the GTN model the yield condition is described by Eqn. (1).

$$\Phi = \left(\sigma_{eq}^{\ 2}\right) / \left(\sigma_{y}^{\ 2}\right) + 2 f^{*} q_1 \cosh\left(\left(3 q_2 p\right) / \left(2\sigma_{y}\right)\right) - \left[1 + \left(q_1 - f^{*}\right)^2\right] \tag{1}$$

where σ_{eq} is the von Mises equivalent stress, p is the hydrostatic stress on a mesoscopic scale, σ_y is the yield stress of the fully dense matrix material as a function of the equivalent plastic strain in the matrix, f^* is the damage parameter, q_1 and q_2 are material parameters for modeling low void volume fractions. The parameter q_1 was introduced to improve the Gurson model for small values of the void volume fraction. For solids with periodically spaced voids, numerical studies have shown that q_1=1.5 and q_2=1 give reasonably accurate results. Based on the description proposed by Needleman (Needleman and Tvergaard 1984), the void volume fraction f in the flow function was replaced by the modified void volume fraction f^*. By introducing this f^* parameter, the rapid decrease in load-bearing capacity can be modelled when void merging occurs.

$$f^* = \begin{cases} f & \text{if } f \le f_c \\ f_c + \left(\dfrac{f_u^* - f_c}{f_f - f_c} \right) (f - f_c) & \text{if } f > f_c \end{cases} \tag{2}$$

where f_c is the critical void volume fraction, f_f is the void volume fraction at failure and f_u^* is the reciprocal of q_1. The void fraction varies with the growth of existing voids and the formation of new voids and can be written as:

$$\dot{f} = \dot{f}_g + \dot{f}_n \tag{3}$$

where $\dot{f}_g$ is the change due to the growth of existing voids and $\dot{f}_n$ is the change due to the nucleation of new voids. The void growth can be determined from the compressibility of the matrix material surrounding the void. Thus, $\dot{f}_g$ is based on the law of conservation of mass and can be expressed using the void ratio:

$$\dot{f}_g = (1 - f)\dot{\varepsilon}_{kk}^{pl} \tag{4}$$

where $\dot{\varepsilon}_{kk}^{pl}$ denotes the plastic volume strain rate.
The formation of new voids can be considered as deformation- or stress-driven. Both follow a normal distribution around a mean value. For deformation-driven nucleation can be described as follows:

$$\dot{f}_n = \frac{f_n}{S_n \sqrt{2\pi}} S \exp\left[-\frac{1}{2} \left(\frac{\varepsilon_m^{pl} - \varepsilon_n}{S_n} \right)^2 \right] \dot{\varepsilon}_m^{pl} \tag{5}$$

where f_n is the volume fraction of void nucleation, ε_n is the mean strain for nucleation, S_n is the standard deviation, which will be larger if the particle size of the second phase in the material varies greatly than if the particle size is more uniform and finally $\dot{\varepsilon}_m^{pl}$ is the effective plastic strain.
Based on this the Gurson-Tvergaard-Needleman model contains eight parameters, which can be given in simplified form as follows:

$$\Phi = \Phi\left(q_1, q_2, f_0, f_c, f_n, f_f, \varepsilon_n, S_n \right) \tag{6}$$

The Gurson parameters listed above for a given material can be determined as follows.

- Initial void volume fraction, f_0: It gives the initial void volume fraction of inclusions in the material that are not strongly bound to the matrix. It can be determined by scanning electron microscopy (SEM) metallurgical examination and validated by examination of notched tensile specimens.
- Critical void volume fraction, f_c: Its value can be determined by fitting the numerical calculations to the measurement results (notched tensile test specimen displacement load or cross-sectional contraction load curve).
- Volume fraction for void nucleation, f_n: It can be determined by metallographic studies or by fitting numerical analysis data to experimental data.
- Failure void volume fraction, f_f: It is determined by metallographic tests. Its value has no significant influence on the parameter fit. The recommended value is between 0.1 and 0.2.
- Mean strain for nucleation, ε_n: It can be determined from tensile testing and metallographic examination; however it is a very difficult procedure.
- Standard deviation, S_n: The nucleation process follows a statistical distribution. Chu and Needleman (1980) have proposed a Gaussian distribution for the instantaneous volume fraction of cavities produced with different deformation values. The S_N is usually taken to be 0.1 for steels but has no significant effect on the results of the tests.

– Yield surface multipliers, q_1=1.5, q_2=1.0 and q_3=2.25(=q_1^2). These values are not usually changed, but some studies suggest that these parameters are also material dependent [9][10].

APPLICATION OF ANN METHOD FOR THE DETERMINATION OF GTN PARAMETERS

To determine the optimal GTN damage parameters for the 15H2MFA material, an artificial neural network (ANN) was constructed and trained using data obtained from finite element simulations. For this purpose, small, notched test specimens were developed, the results of which were fitted with the force-displacement curve from the finite element simulation to determine the Gurson-Tvegaard-Needleman damage parameters. The test specimens were prepared from a 15H2MFA based broken SENB specimen. From this, 8 specimens with parallel test sections and 3x2 specimens with notched flat test pieces were obtained. For the notched specimens, 3 different notch radii were used, with radius of 1, 2 and 4 mm (Fig. 1 left). The right side of Fig. 1 shows the dimensions of the 2 mm radius specimen. The specimens with parallel side were used to determine the flow curve of the material.

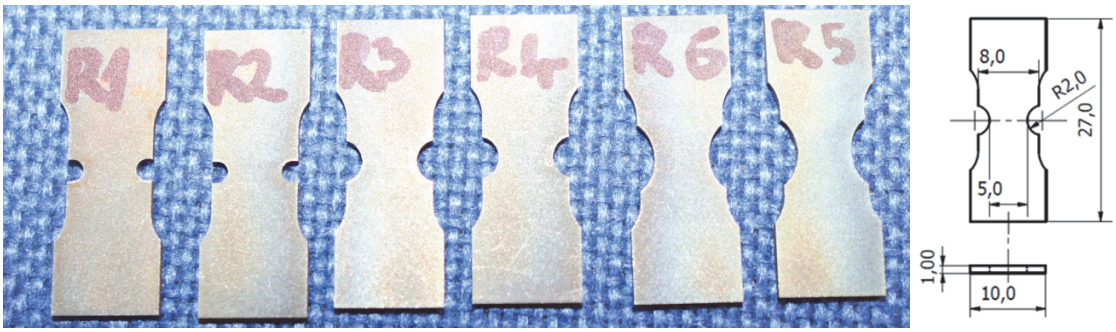

Figure 1: Small flat notched tensile specimens (left), Dimensions of notched flat tensile specimen (right).

The chemical composition of the 15H2MFA austenitic steel is given in Tab. 1.

C	S	P	Mn	Cr	Si	Ni	Cu	As	V	Mo	Co
0.13-0.18	≤0.02	≤0.02	0.3-0.6	2.5-3.0	0.17-0.37	≤0.4	≤0.3	≤0.04	0.25-0.35	0.6-0.8	≤0.025

Table 1: Chemical composition of 15H2MFA.

The tensile tests aimed to determine the strength and deformation properties of the test materials. The tests were carried out using an Instron E10000 uniaxial electrodynamic materials testing machine. Surface deformations were recorded by the GOM 3D optical measuring system and the results were subsequently evaluated using the GOM Correlate 2017 software. During the measurement, the flash cameras track the black and white pattern of the specimen surface - also shown in Fig. 2 - with individual dye points, and the deformation of the specimen can be determined from the displacement of the dye points relative to each other.

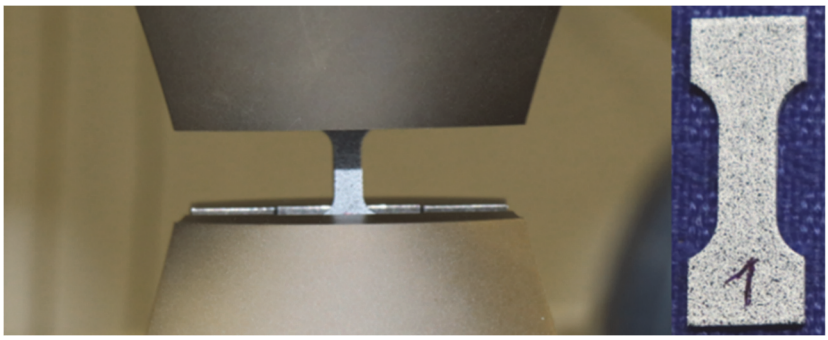

Figure 2: The clamped specimen and the unique pattern on its surface.

Once the yield strength (523 MPa) was determined from the specimens with parallel sides, a finite element simulation of the notched tensile test specimens could be prepared. The resulted true stress-plastic strain curves are shown in Fig. 3. Later in the simulation the averaged version of it was used.

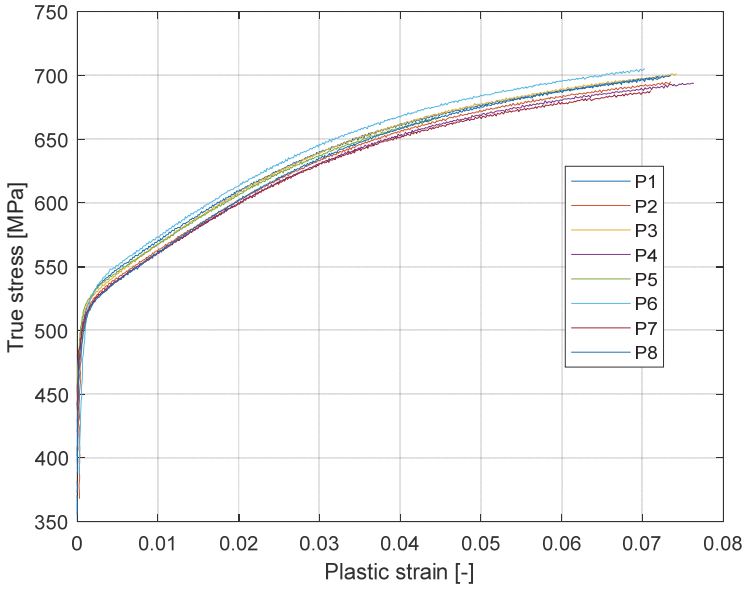

Figure 3: Flow curves obtained from the tensile test.

Note that all the finite element simulations presented in the following have been performed in MSC.Marc Mentat software. The material properties of 15H2MFA steel were set for all models. The modulus of elasticity was set to 203 GPa and the Poisson's ratio was 0.3. Quarter models were used in the calculations to take advantage of the symmetry, meaning that both longitudinal and transverse symmetry were assumed. An element size of 50 μm was used in the crack environment.
Fig. 4 shows the boundary conditions applied to the model of notched tensile specimens. Due to symmetry, degrees of freedom were constrained in x (sym_x), y (sym_y) and z directions (sym_z), and the load (load_x) was defined on the specimen's clamping section, to which the surface nodes were linked to a point.

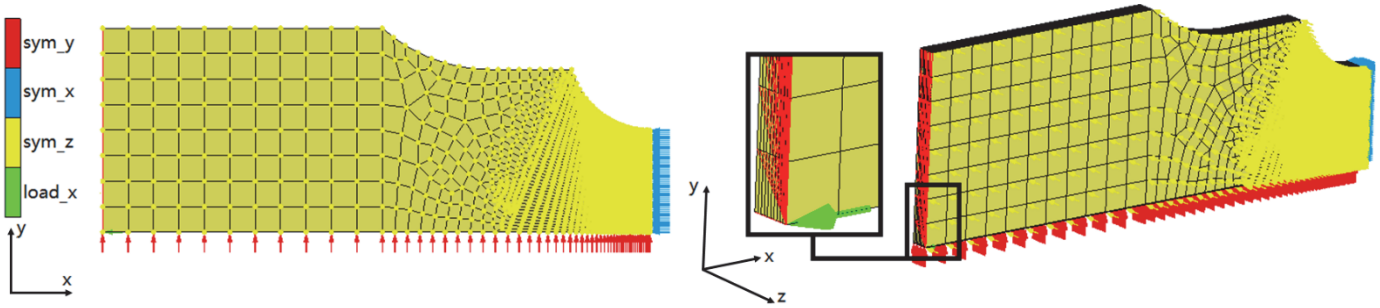

Figure 4: Boundary conditions applied to small notch flat specimens.

The next step is the determination of the GTN parameters, which can be considered as an optimization process where the objective function is to fit the force-displacement curve from the measurement to the results obtained from the simulation. The variables are the GTN parameters, and the constraints are applied to these values. This requires several subtasks to be performed. First, finite element simulations are required, as the input data are provided by the results of these simulations. The second step is to use this data to train the ANN program. During this process, the input data can be generally divided into three groups: training, validation, and verification, however, since the Bayesian regularization method is used, the validation domain is included in the training set. It is important to note that the number of neurons in the hidden layer should be set to a value between the input and output parameter numbers, but it may exceed these numbers, but care must be taken that the program should not generalize the results. In this case, both the input and output parameter sets were between -1 and 1, so scaling them was not necessary. Finally, after training, the goodness of training can be checked using

a previously isolated data set. If these are within a given error range, the network can be simulated with the measured data, from which the GTN parameter set for the material can be determined.
From the above, in the first step, it is necessary to specify a matrix of damage parameters in order to generate the input data set. During the optimization process, these ranges represent the constraints. For this purpose, a range for each GTN parameter was defined based on the literature. Among the GTN parameters, q_1, q_2 and S_n (variance) were given fixed values, thus changing a total of 5 parameters in the optimization task.
Eight force-displacement data pairs were selected to compare the simulated and experimental force-displacement curves. Since the force-displacement curve is relatively horizontal in the region where the GTN parameters affect the curve, displacement values were taken for given force values.

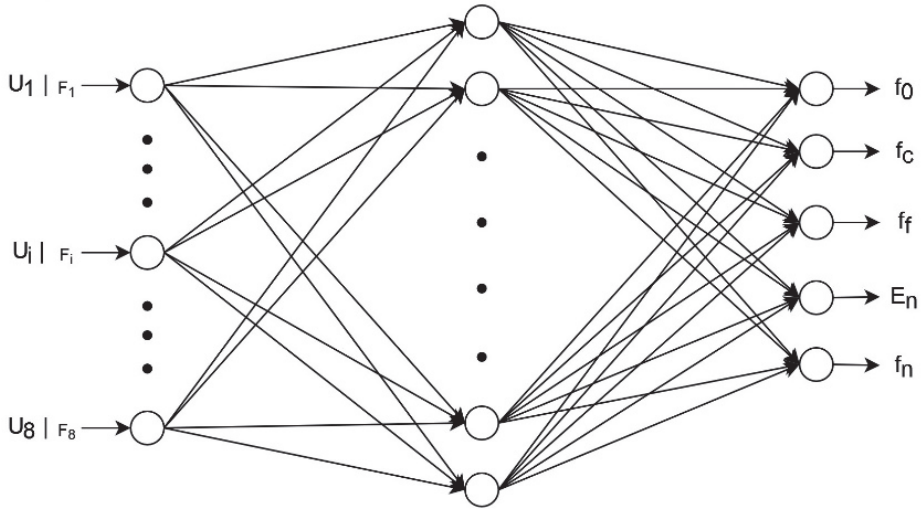

Figure 5: Built-up of artificial neural network.

The usage of the ANN to determine the optimal GTN parameters was introduced in more detail in reference [11] and [12], here only the most important information are included. Two-layer feedforward network with sigmoid hidden neurons and linear output neurons was used. As the data complexity is simple only one hidden layer was applied. The ANN was cross validated; thus the 90 sample was split into training and testing sets.
The neurons in the input layer correspond to the displacements associated to the chosen 8 forces. 8 values were chosen to describe sufficiently the force-displacement curve. The size of the output layer was fixed as the neurons in the output layer represent the damage parameters to be identified (f_n, f_c, f_f, ε_n, f_n). The number of hidden neurons is commonly chosen close to the number of input data. To determine the correct number of hidden neurons, a trial-and-error approach was used. For different numbers of hidden neurons, the ANN was trained ten times, and the value of the errors was calculated. Then, for the final ANN, the smallest number of hidden neurons that still gave satisfactory results was chosen. The ANN (8-6-5) has a structure consisting of 8 neurons in the input layer, 6 neurons in the hidden layer and 5 neurons in the output layer. The build-up of the artificial neural network is shown in Fig. 5.
Finally, the optimized GTN parameters are listed in Tab. 2.

Name	Parameter	Value range
Yield surface multiplier	q_1	1.5
Yield surface multiplier	q_2	1
Initial void volume fraction	f_0	0.0008
Critical void volume fraction	f_c	0.1591
Failure void volume fraction	f_f	0.4035
Mean strain for nucleation	ε_n	0.1803
Standard deviation	S_n	0.05
Volume fraction for void nucleation	f_n	0.0099

Table 2: Optimized values of GTN parameters.

APPLICATION OF DAMAGE PARAMETERS DETERMINED BY ARTIFICIAL NEURAL NETWORKS ON SENB TEST SPECIMENS

The GTN parameters given in Tab. 2 were already validated with the results of 1T CT specimens which were introduced in [11] while the analysis done with 0.16T CT was presented in reference [12]. However, if we have only 0.16CT test, the dimensional response of the parameters can not be investigated, also with only CT geometry, only one type of restricted deformation state can be investigated, which may pose problems in verifying geometry independence and determining local parameters for state-of-the-art analyses. Therefore, normal and mini SENB specimens were also prepared which has a different restricted deformation. The mini SENB can be prepared from the Charpy specimens used in the reactor pressure vessels. The measurements thus made can provide sufficient information to determine the parameters of local models. In the followings, the procedure of the measurements and the simulations are going to be introduced.

Measurements of mini and normal SENB specimens

For fracture mechanics tests, 8 mini SENB specimens were prepared from the 15H2MFA material, but only 4 specimens were successfully preloaded and tested. The length of the specimen is 22 mm, the width is 4.5 mm and the height is 5 mm, the dimensions of the specimen are shown on the right side of Fig. 6. The tests were carried out on Instron E10000 material testing machine according to ASTM E1820-20 [13]. Before testing, a pre-crack was created on the notched specimens by fatigue. The final length of the pre-cracks had to be between 0.45W and 0.55W, where W is the height of the specimen. The crack opening was measured with an Epsilon 3541-003M-025M-LT crack opening extensometer and the load displacement was measured with an Epsilon 3540-012M-LHT deflection extensometer.

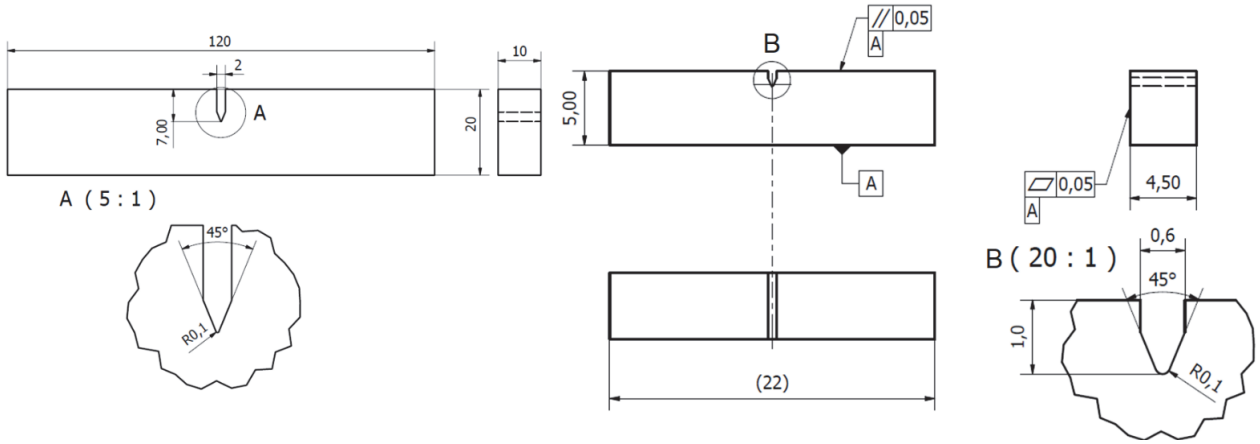

Figure 6: Dimensions of standard (left) and mini (right) SENB test specimens.

Three normal SENB test specimens were prepared from the 15H2MFA material. The dimensions of the specimen were 120x20x10mm (Fig. 6 left). The tests were carried out on an Instron 8803 materials testing machine according to ASTM E1820-20. A pre-crack was created on the notched specimens by fatigue. The crack opening was measured with an Epsilon CP100856 crack opening extensometer and the displacement in the direction of loading was recorded by the machine. After the tests of mini and normal SENB specimens, the pre-crack (a_0) and ultimate crack (a_p) sizes were measured on each specimen at 9 points according to ASTM E 1820-20 [13]. The layout of the mini and standard SENB specimen fracture mechanics tests is illustrated in Fig. 7.

Finite element model of SENB specimens

For the simulation of mini SENB test, a finite element mesh with the inclusion of the Gurson damage model was generated which is shown in Fig. 8. Due to the symmetry, it was possible to use a quarter model where the missing geometry was taken into account using boundary conditions. A denser mesh was required in the vicinity of the load and support rollers, as well as in the region of the pre-cracking and the crack propagation direction.

The mesh size in the crack region is 50 μm, the model contains 62160 hex(8) elements and 68589 nodes. Along with the thickness, the damage model requires more elements in the environment of the crack propagation. To lower the computational capacity and time, larger elements were created as the distance from this region increased. The aim was to

have the same element size in all three directions in the path of the damage propagation. The shape of the pre-crack used for the validation of the mini SENB damage parameters was set to the dimensions obtained from the tested specimens.

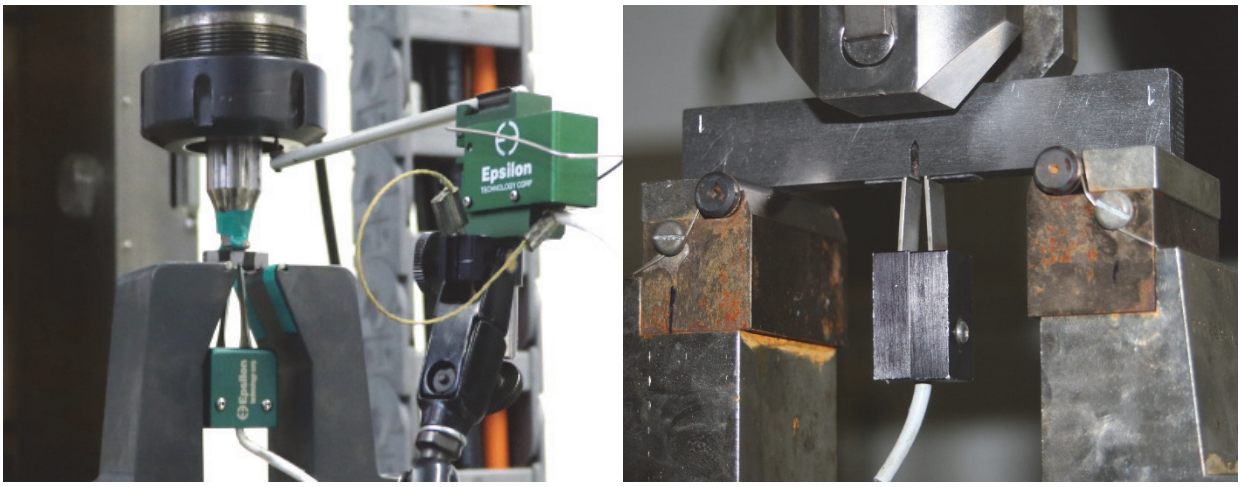

Figure 7: Mini (left) and standard (right) SENB test specimen fracture mechanics test set-up.

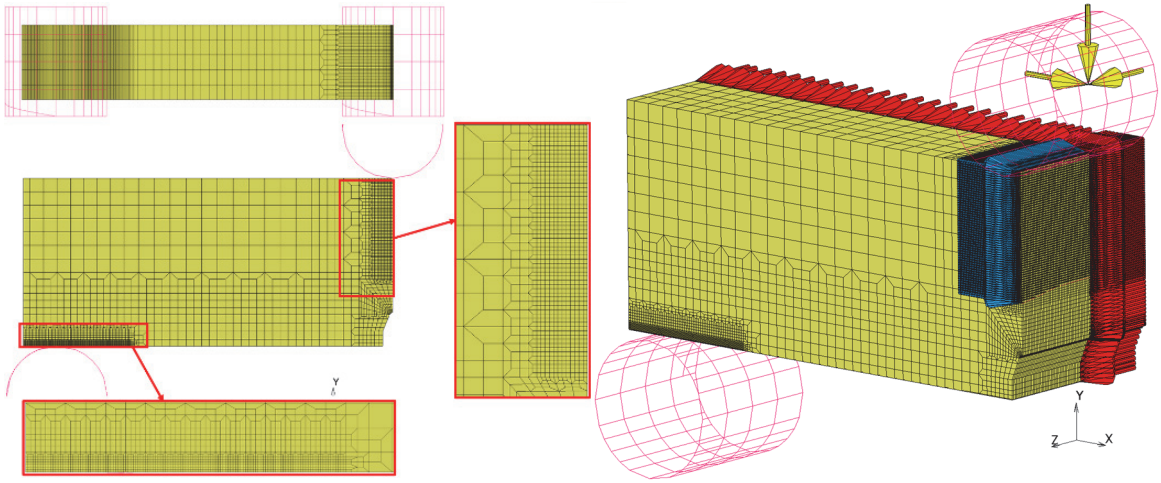

Figure 8: Mini SENB specimen finite element mesh for damage model (left), boundary conditions – yellow: load, blue: longitudinal symmetry, red: symmetry along thickness (right).

During the generation of the finite element mesh of the normal SENB specimen, the same assumptions were taken into account as in case of the miniaturized version. The arrows marked with red and yellow ensure the symmetry along the length and thickness of the specimen, while the blue arrows indicate the displacement of the load roller, which is not allowed to move in the thickness and length directions, nor is the roller allowed to rotate along any axis. All degrees of freedom of the support roller are limited. The support and load rollers were simulated as rigid bodies and a touching contact was set between them and the flexible specimen. The mesh generated for the model and the locations of the boundary conditions are shown in Fig. 9.

Elastic-plastic material model was chosen for the simulation where for the elastic material properties Young's modulus was set to 203 GPa and the Poission's ratio to 0.3. The flow curve was obtained from the 8 specimens with parallel sides.

Validation of GTN parameters

The validation of the GTN parameters was performed on the mini and normal CT and SENB specimens. In the followings, the results of SENB simulations are going to be introduced, the results of CT specimen were shown in reference [11] and [12]. In case of the mini specimen in reference [12] it was already shown that the real geometry dimensions of the pieces and the real pre-crack shape has some impact on the final force-displacement curves, therefore this effect in case of the mini SENB specimen was also checked. Fig. 10 shows the pre-crack of the specimen. In the first version the measured

values were averaged, which is a common procedure in case of normal sized specimens, and the simulation was carried out with this pre-crack length, here the theoretical dimensions of the specimen was used (Fig. 6 right). In the second version the pre-crack shape was simplified for half geometry to take it into account to some extent.

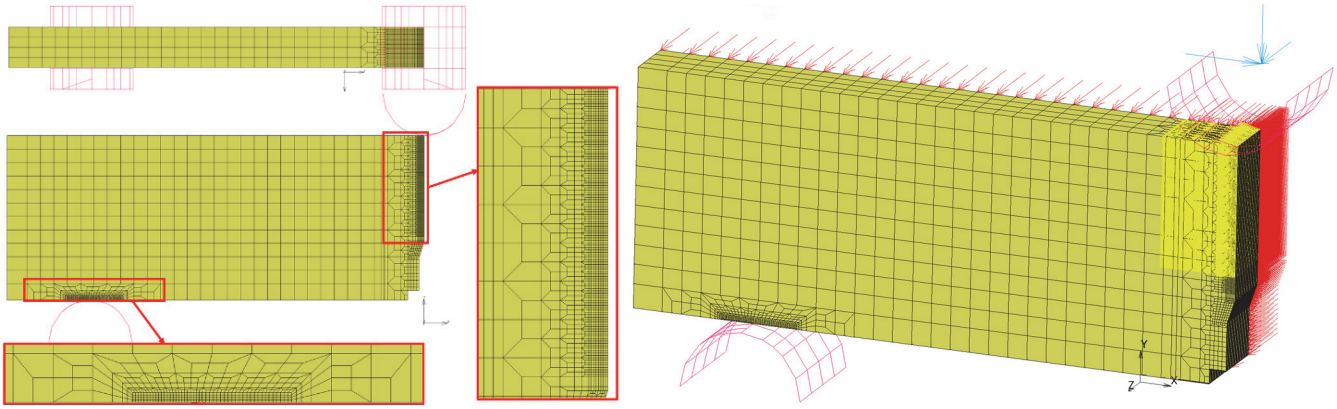

Figure 9: normal SENB specimen finite element mesh for damage model (left), boundary conditions – blue: load, yellow: longitudinal symmetry, red: symmetry along thickness (right).

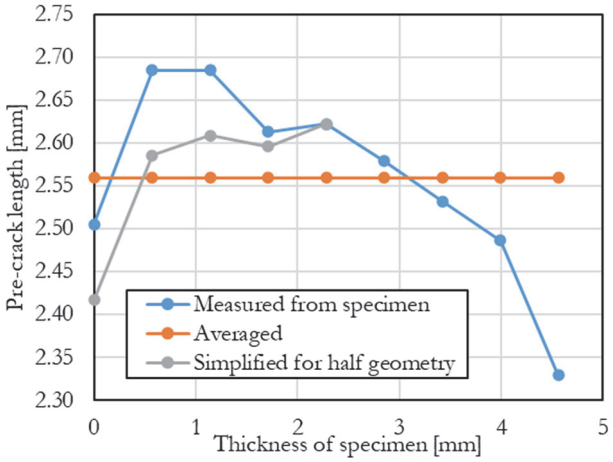

Figure 10: Pre-crack length as a function of the thickness.

In case of the mini SENB specimens, the force is illustrated as a function of crack opening displacement (COD). The results obtained from the test and simulations are compared in Fig. 11, both in terms of the force-displacement curve, which include both simulation cases and crack propagation (fracture surface) where only the shape obtained from the real geometry and pre-crack shape are compared. The results show that the simulation with the real geometry dimensions and the simplified version of the real pre-crack shape is in very good agreement with the measured force-COD curve, while the simulation with the theoretical sizes and averaged pre-crack length has some deviation from the measured curve. It also can be concluded that, the damage parameters defined with ANN are appropriate for the 15H2MFA material, as when applied to a fracture mechanics test specimen with different geometry, the simulation results show good agreement with the measured data.

The usage of the real dimensions and pre-crack shape is not necessary in the case of the normal specimens, therefore for the generation of the mesh the dimensions given on the technical drawing was used, and an averaged value was applied for a_0. For the normal SENB test specimen, the averaged pre-crack size was set in the model, giving the result shown in Fig. 12. Here, the effect of the shape of the pre-crack was less significant. It can be seen that the simulations with the determined GTN parameters are in very good agreement with the test results. However, it should be noted that these parameters are element size dependent therefore they can only be used when in the region of crack propagation is 50 μm. With this, the geometry independence and the method of the determination of local parameters for state-of-the-art analyses was verified, as for both restricted deformations state the GTN parameters worked well.

In the simulations, it was found that the small-size specimens (mini SENB, mini CT) were more sensitive to geometric dimensions and also to the size and shape of the pre-cracking, which were not present in the normal-size specimens.

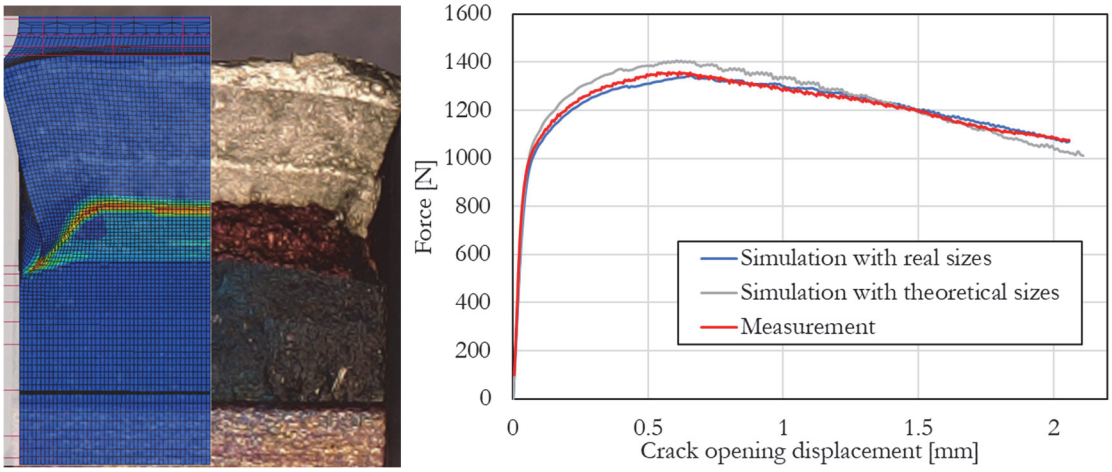

Figure 11: Fracture surface (left) and force-COD diagram (right) of mini SENB test specimens.

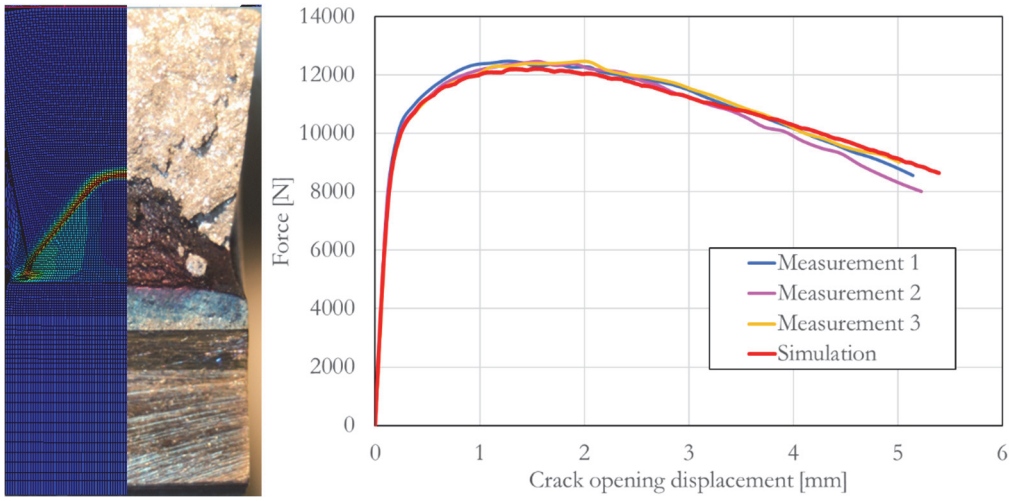

Figure 12: Fracture surface (left) and force-COD diagram (right) of normal SENB test specimens.

IMPLEMENTATION OF THE MODIFIED VCCT METHOD FOR THE SIMULATION OF SENB SPECIMENS

Built-up of 2D finite element model

In order to determine the goodness of fit of the developed model, a 2D finite element model of the normal-size SENB specimen was constructed. The VCCT method requires a predefined crack path limited to the element boundaries. The modified finite element model of the standard SENB test specimen is illustrated in Fig. 13. A 2D plane-strain model with linear four-node elements was used in the simulations, while the rollers were assumed to be perfectly rigid. A displacement in the vertical direction was given at the center of each of the two pins, while the displacement in the horizontal direction was fixed. Finally, to ensure that the model could not move in the direction perpendicular to the force, gripping along the plane of symmetry of the specimen was applied at the nodes as illustrated in Fig. 13. The mesh of the mini SENB specimen was generated the same way as it was already introduced in case of the normal SENB and it is shown in Fig. 14. Experience has shown that for small specimens, contact surfaces should be taken into account as they have a large influence on the results obtained. If the loading is applied along a point, the application of the damage model will cause locally large deformations at the point of contact during the calculation, which will damage the material at this location, essentially

causing a numerical error in the simulation, and thus the results will be inconsistent with the measurement. Therefore, the shape of the load roller pin has been taken into account during the generation of mesh.

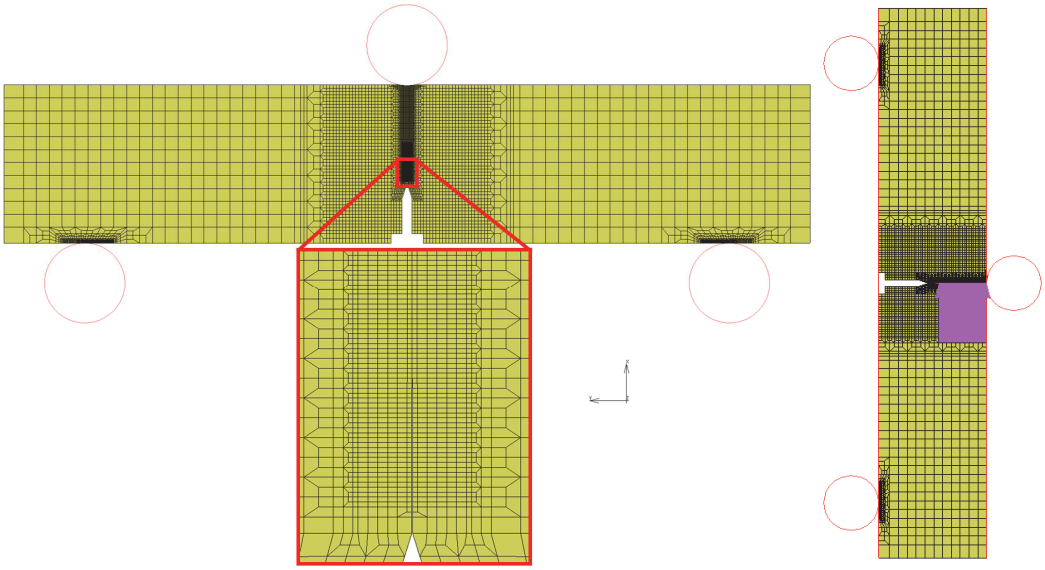

Figure 13: 2D mesh of the normal SENB specimen (left), symmetry boundary condition.

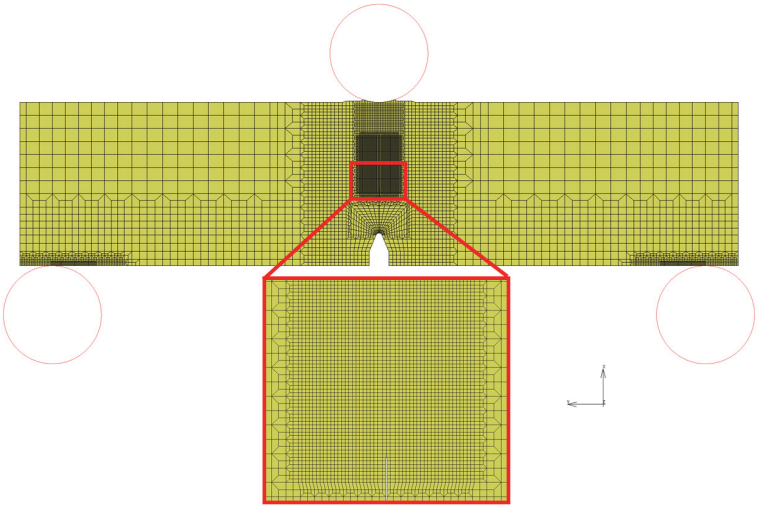

Figure 14: 2D mesh of the min SENB specimen.

Evaluation of results with ASME E1820-20

The ASTM E1820, "Standard Test Method for Measurement of Fracture Toughness" standard [13] provides procedures and guidelines for the determination of fracture toughness of metals using various fracture parameters (stress intensity factor K, J-integral and crack tip opening displacement δ). This test method is primarily used to conduct and analyse elastic-ductile fracture toughness tests to characterise the resistance of a material to crack propagation, where the critical parameter is the J-integral used at (or near) the onset of stable crack propagation.

In E1820-20b, two approaches are used to characterise the fracture toughness of metallic materials, multiple specimen technique and single test specimen technique. Of the two versions, the second method was used for both the mini and the standard SENB specimens. In this method, the crack propagation is inferred by measuring the specimen compliance by applying small loads (less than 15 % of the maximum force) at regular intervals during the test. In this way, the number of loadings is equal to the number of data points on the resistance (J-R) curve. The slope (expressed in terms of displacement/force ratio) of these loads can be analytically related to the crack size for standard specimen geometries.

Fracture toughness was determined in the following cases.

- Evaluation of test results for mini and normal SENB specimens.
- 2D load simulation, using a modified VCCT method, from which the fracture toughness value is determined according to ASTM E1820-20.
- Unloaded 2D simulation using a modified VCCT method, from which the fracture toughness value is determined directly from the simulation.

An important applicability criterion of the standard is that a minimum of 8 points or a correlation factor of at least 3 points between $0.4J_Q$ and J_Q or a correlation factor of more than 0.96 is required to determine the initial predicted crack size (a_{0q}). In addition, if the optically measured crack size, a_0, differs from a_{0q} by more than 0.01W or 0.5 mm, the data set is not satisfactory according to this test method.

Fig. 15 shows the evaluation results of the measured normal SENB specimen according to ASTM E1820-20. The number of validated points exceeded 8 and at least one measurement result fell between the 1.5 mm and 2.0 mm construction lines. In this case, the value of J_Q was found to be 446.70 kJ/m². Note that the relative standard deviation of the material properties related to the crack propagation resistance of the materials (K_{IC}, J_{IC}) is a "coefficient of variance" (standard deviation/expected value×100) of 10% or more. However, the experimental work is based on the intersection of these values with different curves, so two-tenths order of magnitude was used in order to make more accurate comparisons.

Fig. 16 shows the evaluation results of 2D normal SENB specimen simulations according to ASTM E1820-20. In this case, the value of J_Q was found to be 443.12 kJ/m².

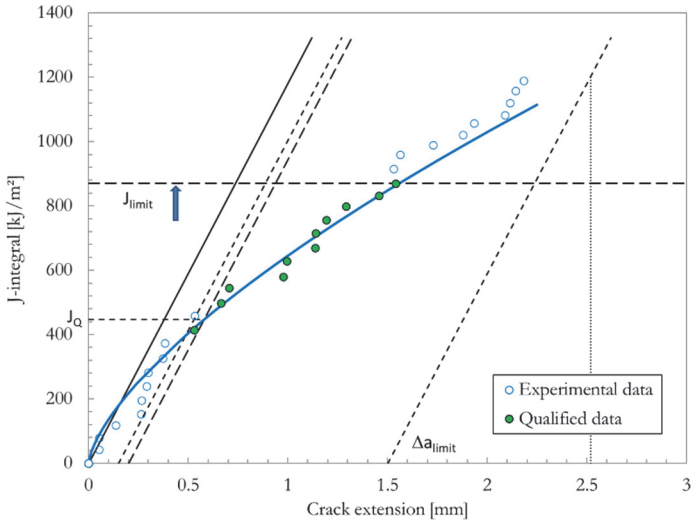

Figure 15: Evaluation of standard SENB measurement results according to ASTM E1820-20.

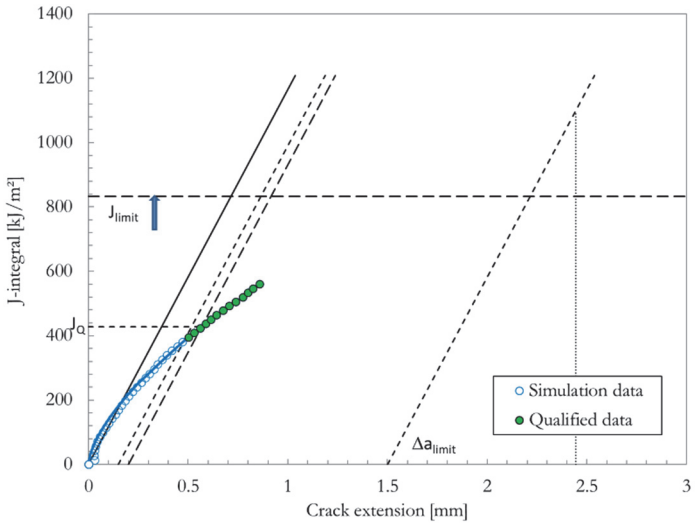

Figure 16: Evaluation of standard SENB 2D simulation results according to ASTM E1820-20.

Comparison of results of miniaturized and normal SENB specimens

The fracture toughness values achieved from the SENB specimens are summarized in Tab. 3. In case of the normal SENB specimens the measured and the simulated fracture toughness results are in good agreement, and the deviation is less than 2%.

Type of specimen	Origin of data	Analyzing method	Fracture toughness (kJ/m²)	Difference
Normal SENB	Measurement	ASTM E1820-20	446.70	-
	Simulation with VCCT		443.12	-0.8%
	Simulation with VCCT	Simulation	439.62	-1.58%
Miniaturized SENB	Measurement	ASTM E1820-20	384.84	-
	Simulation with VCCT	Simulation	327.77	-14.83%

Table 3: Fracture toughness results.

Unfortunately, in case of the miniaturized SENB the value of J_Q is not valid based on the ASTM E1820-20 (2020) standard, therefore the differences are higher between the normal and the miniaturized SENB results (around 17%) than the deviations resulted from the miniaturized CT specimens in reference [12]. Furthermore, in case of the 2D simulations, it was not taken into account how the real shape of the initial crack effects the force displacement curve during the calculation.

SUMMARY

2D and 3D nonlinear FE analysis was performed to study the ductile fracture in the SENB test specimen. The GTN fracture model was adopted to describe the ductile crack growth. The predictability of the proposed method was evaluated and verified through the prediction of the ductile fracture pattern and the force-crack opening response. The parameters of the GTN model were calibrated using uniaxial tensile test data of 15h2MFA steel from the material plate used in this research work. Secondly, the force-crack opening displacement experimental data of the SENB test were simulated on standard and miniaturized specimens with a/W=0.5 pre-cracking. The good agreement between the simulations and the uniaxial tensile and SENB tests suggests that the GTN fracture model with well-calibrated material parameters can provide reliable predictions of ductile fracture of structural alloys. Finally, the calibrated GTN model was applied to modified VCCT simulations of SENB specimens. For normal SENB specimens, the measured and simulated fracture toughness results show excellent agreement. In contrast, it was found that the agreement was not as good for the miniature SENB specimen, and further investigation is needed to determine the reason for this.

REFERENCES

[1] Das, A., Chekhonin, P., Houska, M., F. Obermeier, Altstadt, M. (2023). Master curve testing of RPV steels using mini-C(T) specimens – Irradiation effects and censoring statistics, Nuclear Materials and Energy, 34. DOI: 10.1016/j.nme.2023.101395.

[2] Chen, B., Yongduo, S., Yuanjun, W., Kaiqing, W., Li, W., Guangwei, H. (2021). Fracture properties and crack tip constraint quantification of 321/690 dissimilar metal girth welded joints by using miniature SENB specimens, Nuclear Engineering and Technology, 53(6), pp. 1924-1930. DOI: 10.1016/j.net.2020.12.020.

[3] Gurson, A. L. (1977). Continuum Theory of Ductile Rupture by Void Nucleation and Growth: Part I--Yield Criteria and Flow Rules for Porous Ductile Media, Journal of Engineering Materials and Technology, 99(1), pp. 2-15. DOI: 10.1115/1.3443401

[4] Needleman, A., Tvergaard, V. (1984). An analysis of ductile rupture in notched bars, Journal of the Mechanics and Physics of Solids , 32(6), pp. 461-490. DOI: 10.1016/0022-5096(84)90031-0

[5] Corigliano, A. (2003). 3.09 – Damage and Fracture Mechanics Techniques for Composite Structures, Comprehensive Structural Integrity, pp. 459-539. DOI: 10.1016/B0-08-043749-4/03041-X

[6] Pineau, A. (1992). Global and local approaches of fracture - transferability of laboratory test results to components. In Topics in Fracture and Fatigue, pp. 197-234. DOI: 10.1007/978-1-4612-2934-6_6.
[7] Lindqvist, S., Dahl, A., Smith, M., Blouin, A., Dillström, P., Nicak, T., Forsström, A. (2022) Final project report - ATLAS+ (Advanced Structural Integrity Assessment Tools for Safe Long Term Operation): D6.9-21. (V2 ed.) ATLAS+ project
[8] Blouin, A., Marie, S., Remmal, A.M. (2019) ATLAS+ European Project: Prediction of Large Ductile Tearing in Piping Using Local Approach. Proceedings of the Volume 6A: Materials and Fabrication. San Antonio, Texas, USA. July 14–19, 2019. V06AT06A047. ASME. DOI: 10.1115/PVP2019-93586
[9] Achouri, M., Germain, G., Santo, P. D., Saidane, D. (2013). Experimental characterization and numerical modeling of micromechanical damage under different stress states. Materials & Design, 50, pp. 207–222. DOI: 10.1016/j.matdes.2013.02.075.
[10] Yan, R., Xin, H., Veljkovic, M. (2019). Identification of GTN damage parameters as a surrogate model for S355. In Proceedings of the 17th International Symposium on Tubular Structures (ISTS17). Research Publishing Services. DOI: 10.3850/978-981-11-0745-0_066-cd.
[11] Bézi, Z., Spisák, B., Erdei, R., Szávai, Sz. (2023). Simulation of crack propagation using a GTN ductile damage model based on the virtual crack closure technique, Procedia Structural Integrity, 47(3), pp. 646-653. DOI: 10.1016/j.prostr.2023.07.057.
[12] Bézi, Z., Spisák, B., Erdei, R., Szávai, Sz. (2023). Modification of VCCT method with implementation of GTN model for the determination of J-integral, Procedia Structural Integrity 48(10), pp. 326-333. DOI: 10.1016/j.prostr.2023.07.125
[13] ASTM E1820-20 (2020). Standard Test Method for Measurement of Fracture Toughness.